Published in final edited form as:
Pflugers Arch. 2013 September ; 465(9): 1327–1340. doi:10.1007/s00424-013-1264-6.

Visualization of fast calcium oscillations in the parafascicular nucleus

James Hyde[1], **Nebojsa Kezunovic**[1], **Francisco J. Urbano**[2,#], and **Edgar Garcia-Rill**[1,#]

[1]Center for Translational Neuroscience, Department of Neurobiology & Dev. Sci., University of Arkansas for Medical Sciences, Little Rock, AR, USA.

[2]IFIBYNE, CONICET, University of Buenos Aires, Buenos Aires, Argentina.

Abstract

The parafascicular nucleus (Pf) is an ascending target of the pedunculopontine nucleus (PPN) and is part of the "non-specific" intralaminar thalamus. The PPN, part of the reticular activating system, is mainly involved in waking and rapid eye movement (REM) sleep. Gamma oscillations are evident in all Pf neurons and mediated by high threshold voltage-dependent N- and P/Q-type calcium channels. We tested the hypothesis that high-speed calcium imaging would reveal calcium mediated oscillations in synchrony with patch clamp recorded oscillations during depolarizing current ramps. Patch-clamped 9 to 19 day old rat Pf neurons (n = 148, dye filled n = 61, control n = 87) were filled with Fura 2, Bis Fura, or Oregon Green BAPTA-1. Calcium transients were generated during depolarizing current ramps and visualized with a high-speed, wide-field fluorescence imaging system. Cells manifested calcium transients with oscillations in both somatic and proximal dendrite fluorescence recordings. Fluorescent calcium transients were blocked with the nonspecific calcium channel blocker, cadmium, or the combination of ω- Agatoxin-IVA (AgA), a specific P/Q-type calcium channel blocker and ω-conotoxin-GVIA (CgTx), a specific N-type calcium channel blocker. We developed a viable methodology for studying high-speed oscillations without the use of multi-photon imaging systems.

Keywords

Arousal; gamma band activity; intralaminar thalamus; P/Q-type channels

Introduction

Gamma band oscillations in the cortex appear to participate in sensory perception, problem solving, and memory [8, 12]. Cortical interneurons can generate gamma oscillations through the activation of subthreshold oscillations subserved by voltage-dependent, persistent sodium channels [25], while in thalamocortical neurons in "specific" thalamic nuclei, the mechanism responsible for gamma band activity involves high threshold, voltage-dependent P/Qtype calcium channels, which were localized to the dendrites of these neurons using calcium imaging [33]. Recently, we described the presence of gamma band activity in nuclei of the reticular activating system (RAS), specifically, the pedunculopontine nucleus (PPN) [23], and the "nonspecific" intralaminar thalamic parfascicular nucleus (Pf) [22]. The role of gamma band activity in these regions was proposed, rather than participating in sensory

Corresponding author: E. Garcia-Rill, PhD, GarciarillEdgar@uams.edu, Tel 501-686-5167, Fax 501-526-7928, Director, Center for Translational Neuroscience, University of Arkansas for Medical Sciences, 4301 W. Markham St., Slot 847, Little Rock, AR 72205.
[#]contributed equally as last authors

None of the authors have a conflict of interest.

binding, to be involved in the process of preconscious awareness [10, 44]. The mechanism behind both PPN and Pf gamma band activity was found to be generated by P/Q-type calcium channels [23, 22], however, these channels have never been localized using calcium imaging. The present study was undertaken to determine if high threshold calcium channel-dependent membrane oscillations in Pf neurons are localized to the dendrites.

The parafascicular nucleus (Pf) is considered a major component of the intralaminar thalamus (ILT), which in turn is considered part of the “nonspecific” thalamocortical system. Pf neurons send wide-ranging projections to the cortex, striatum, subthalamic nucleus, and substantia nigra [14, 43]. These neurons have long, sparsely branching processes as opposed to the compact, bushy primary dendrites found in “specific” thalamocortical (TC) and centrolateral (CL) cells [6, 7]. Some TC neurons present in both the “specific” and “nonspecific” systems possess bushy processes and are multidendritic with stereotypical intrinsic properties such as bistable states of tonic *vs* bursting patterns of activity due to the presence of T-current mediated low threshold spikes (LTS) [26]. This bistable mechanism is considered crucial to the cortical synchronization of high frequency rhythms present during waking and REM sleep (tonic pattern), and synchronization of low frequency rhythms during slow wave sleep (SWS) (LTS bursting). *In vivo* electrical stimulation of the CL-Pf nuclei has been shown to generate arousal and gamma band activity (~30–90 Hz) in the cortical EEG [40]. Pf neurons have also been shown to be involved in maintaining consciousness and selective attention in primates [28, 34].

We recently reported that all cells in the pedunculopontine nucleus (PPN, mainly cholinergic afferents to Pf) can fire at gamma band frequencies, but no higher, when depolarizing ramps are applied [23]. Current ramps induced cells to oscillate at gamma band frequencies through specific calcium (depolarizing phase of the oscillation) and potassium (repolarizing phase of the oscillation) channels [23]. We also described similar properties in Pf neurons [22]. High threshold P/Q-type calcium channels ($Ca_v2.1$) are present in the dendrites of TC relay neurons. These channels are linked with the generation of gamma band oscillations in the thalamus [24, 33, 36]. P/Q-type calcium channel knockout animals show deficits in gamma band generation [24]. N-type calcium channels ($Ca_v2.2$) are found throughout the central nervous system, and animals lacking N-type calcium channels show deficits in long-term memory and long-term potentiation [18]. Previous work has shown the specific P/Q-type calcium channel blocker, ω-agatoxin-IVA (AgA), completely abolished calcium oscillations in both Pf and PPN neurons. The specific N-type calcium channel blocker, ω-conotoxin-GVIA (CgTx), only reduced calcium oscillation amplitude, indicating that both voltage-dependent P/Q- and N-type calcium channels may mediate the depolarizing phase of gamma band oscillations in both the Pf and PPN [22, 23].

While we have shown the presence of P/Q- and N-type calcium channels in Pf neurons, we have not been able to visually localize these channels. P/Q-type channels are known to be present in the dendrites of “specific” TC relay neurons [33]. The studies include a method for visualizing and analyzing high speed P/Q- and N-type calcium channel-mediated transients in Pf neurons with the goal of determining the properties calcium transients and their spatial characteristics during calcium oscillations. We used a combination of Fura 2, Bis Fura, and Oregon Green BAPTA 1 because each dye is best suited to examining the different aspects of these oscillations. We were interested in ratiometric measures to provide an assessment of calcium levels as well as fast imaging to visualize these rapidly oscillating channels. Furthermore, we used multiple dyes to provide flexibility to different researchers in the scientific community in relating these techniques to their experiments. Our results show a direct correlation between membrane potential gamma band oscillations and intracellular [Ca^{2+}] levels, suggesting that gamma oscillations play a central role in the intracellular second messenger pathways of intralaminar thalamic Pf neurons.

Methods

Slice Preparation

All experimental protocols were approved by the Institutional Animal Care and Use Committee of the University of Arkansas for Medical Sciences, and were in agreement with the National Institutes of Health guidelines for the care and use of laboratory animals. Rat pups aged 8–19 days were taken from adult timed-pregnant Sprague-Dawley rats weighing 350–380 g. Pups were anesthetized with ketamine (70 mg/kg, i.m.) until the tail pinch reflex was absent. Pups were decapitated and the brain was rapidly removed and cooled in oxygenated sucrose-artificial cerebrospinal fluid (sucrose-aCSF). The sucrose-aCSF consisted of (in mM): sucrose, 233.7; $NaHCO_3$26; KCl, 3; $MgCl_2$8; $CaCl_2$0.5; glucose, 20; ascorbic acid, 0.4; and sodium pyruvate, 2. Sagittal sections (400 μm) containing the Pf nucleus were cut under cooled oxygenated sucrose-aCSF with a Leica VT1200S vibratome (Leica Biosystems, Buffalo Grove, IL) with a Huber mini-chiller (Huber, Offenburg, Germany), and allowed to equilibrate in normal aCSF at room temperature for 1 hr. The aCSF was composed of (in mM): NaCl, 117; KCl, 4.7; $MgCl_2$1.2; $CaCl_2$, 2.5; NaH_2PO_4, 1.2; $NaHCO_3$, 24.9; and glucose, 11.5. Slices were recorded at 37°C while being superfused (1.5 mL/min) with oxygenated (95% O_2 and 5% CO_2) aCSF in an immersion chamber. The aCSF contained the following synaptic receptor antagonists: the selective NMDA receptor antagonist 2-amino-5-phosphonovaleric acid (APV; 40 μM), the competitive AMPA/kainite glutamate receptor antagonist 6-cyano-7nitroquinox-aline-2, 3-dione (CNQX; 1 μM), the glycine receptor antagonist strychnine (STR; 10 μM), and the specific $GABA_A$ receptor antagonist gabazine (GBZ; 10 μM).

Whole-cell patch-clamp recordings

Infrared differential interference contrast optics was used to visualize neurons using an upright microscope (Nikon FN-1, Nikon, USA) and QICAM camera (QImaging, Surrey, BC). A 40X, 0.8 numerical aperture (NA) fluorite water immersion objective (Nikon) was used. Whole-cell recordings were performed using borosilicate glass capillaries pulled on a P-97 puller (Sutter Instrument Company, Novato, CA), and filled with EGTA-free, high-K^+ intracellular solution, designed to mimic the intracellular electrolyte concentration, composed of (in μM) K-gluconate, 124; HEPES, 40: Mg-ATP, 4; GTP, 0.4 mM; phosphocreatine, 10; and $MgCl_2$2. The internal solution was supplemented with Ca^{2+} sensitive dyes described below. Osmolarity was adjusted to ~270–290 mOsm and pH to 7.3. The pipette resistance was 2–6 MΩ. Previous work showed that oscillations and membrane characteristics were unaffected by pipette resistance within the range of resistances used [22, 23]. All recordings were made using a Multiclamp 700B amplifier (Molecular Devices, Sunnyvale, CA, USA) in current clamp mode. Series resistance and liquid junction potential were compensated for. The average series resistance was 16.7±0.39 MΩ prior to 35–40% compensation (>14 KHz). Analog signals were low-pass filtered at 2 kHz, and digitized at 10 kHz using the Digidata-1440A interface and pClamp10 software (Molecular Devices). Holding current of <80pA was used to maintain resting membrane potential of −50mV if necessary. The recording region was located immediately anterior and posterior to the middle third of the fasciculus retroflexus (fr). Gigaseal and further access to the intracellular neuronal compartment were achieved in voltage clamp mode, with the holding potential set at −50 mV (i.e., near the resting membrane potential of Pf neurons). Soon after the membrane was ruptured, the intracellular solution and dyes were allowed to equilibrate for 10 min without significant changes in either series resistance (bridge compensation in current clamp mode) or membrane capacitance values before imaging recordings were performed. Experiments lasted between 15 to 25 minutes from breaking into the cell to experiment completion. Calcium mediated activity was studied in current clamp mode, in the presence of synaptic blockers (SB, see above) and tetrodotoxin (TTX; 3 μM). Membrane

potential was depolarized from −50 mV (a membrane potential known to inactivate T-type calcium channels [22,23]) using enough current to elicit oscillations, 400–500 pA, 2 sec duration ramp current protocols.

Drug application

Bath-applied drugs were administered to the slice via a peristaltic pump (Cole-Parmer, Vernon Hills, IL), and a three-way valve system such that solutions reached the slice 1 min after the start of application. The sodium channel blocker tetrodotoxin citrate (TTX, 3 μM) was purchased from Sigma (St. Louis, MO). Channel blockers were purchased from either Peptide International (Louisville, KY) or Alomone Labs (Jerusalem, Israel). We used cadmium chloride (Cd_{+2}100 μM), a non-specific voltage-dependent calcium channel blocker, ω-agatoxin-IVA (AgA; 100–200 nM), a specific P/Q-type calcium channel blocker, and ω-conotoxin-GVIA (CgTx; 1.5–2.5 μM), a specific N-type calcium channel blocker. Blockers were applied for ≥10 min before testing.

Ca^{2+} Indicators

Calcium imaging in the Pf has never been reported. This is the initial report of such imaging and, of necessity, describes a number of different fluorescent dyes and their properties. This information is useful in determining optimal quantum yield, photobleaching and quenching, in addition to cell permeability, lifetime in a living cell, and toxicity. We therefore carried out comparative studies to identify optimal conditions for this new region. A variety of Ca^{2+} sensitive dyes were tested for this study. These included Asante Calcium Red, Fura-2, Bis-Fura-2, Fura-4F, Fura-FF, Indo-1, mag-Indo-1, Fluo-3, Fluo-4, Fluo-8, Oregon Green BAPTA-1, and Oregon Green BAPTA-2. Asante Calcium Red, Indo-1 and mag-Indo-1 were purchased from TEFLabs (Austin, TX). All other dyes were purchased from Invitrogen (Grand Island, NY). Only Fura-2, Bis-Fura-2, and Oregon Green BAPTA 1 (OGB1) were used for this paper. Fura-FF, Fura-4F, mag-Indo-1, and Oregon Green BAPTA-2 showed negligible results due to the lower calcium affinity. Asante Calcium Red was not used due to its low fluorescence emission levels. Indo-1 was not used because of low fluorescence and it failed to perfuse dendrites. OGB1 was selected instead of the Fluo series of dyes due to its stronger fluorescence and fast dynamics. Fura-2 (200 μM), Bis-Fura (200 μM), or OGB1 (200 μM) were loaded with the intracellular solution. Some cells were co-injected with Alexa-594 Hydrazide (Invitrogen, 50 μM) as a volumetric marker.

Ca^{2+} Imaging

Cells were illuminated with a Lambda DG-4 high speed wavelength switcher equipped with a 300W xenon arc bulb (Sutter Instruments). Indicator-filled neurons were visualized at 64×64 pixels with an Evolve 128 EMCCD camera (Photometrics, Tucson, AZ) operating with a 2X bin with a low EM gain (typically ~20X). Fura 2 and Bis Fura exposures were acquired in pairs with exposures of 2.5 msec (400 frames/sec) with ~1.2 msec wavelength switching time. OGB1 image streams were acquired with a single excitation wavelength (480/40×) with 2 msec exposures (500 frames/sec). Image streams were saved continuously in computer ram using Metamorph software (Molecular Devices), and subsequently saved to the hard disk. All imaging and recording synchronization was accomplished through pCLAMP Clampex software. All images were processed in ImageJ [36] where they were background corrected using the EMBL tools plugin with the simple ratio correction method [30], applied a 3D median filter [17], and registered with the Registax plugin [43]. Ratio images were processed with the Ratio Plus plugin. Image stacks were analyzed in Metamorph. A 3x3 pixel region of interest were extracted from each image. Extracted fluorescence recordings were analyzed in OriginPro (OriginLab Corporation, Northampton, MA). OGB1 recordings were detrended in OriginPro.

Calcium calibration was accomplished with a calibration buffer kit from Invitrogen (kit C-3008MP), using protocols outlined by Invitrogen. The kit contains two buffers with 30mM MOPS at pH 7.2 in 100 mM KCl, one buffer with 39 μM free Ca^{2+} and the other with zero free Ca^{2+}. This kit does not perfectly match the intracellular conditions present, but does mimic the osmotic and pH of the intracellular solution used and allows us to confirm the K_d in our system. The kit employs a reciprocal dilution method to minimize indicator concentration errors [21, 42]. Each buffer solution was visualized in our imaging system and fluorescent intensities were recorded.

Confocal Imaging

Upon completing Ca^{2+} imaging, the patch electrode was carefully removed to maintain cell structure. Slices were fixed overnight in 4% paraformaldehyde at 4°C. The slices were then washed with 0.1 M phosphate buffer and mounted with Fluoromount (Sigma). Slices were examined with a Nikon AZ100 multizoom fluorescence microscope to determine suitability for confocal scanning. Intact neurons were scanned on a Zeiss PASCAL LSM 5 confocal microscope (Oberkochen, Germany) with a 40X 0.8NA objective. Alexa-594 was illuminated with 543 nm excitation light. Image stacks were acquired at 1024×1024 with 4X averaging. Stacks were deconvoluted and processed with Amira software (Visualization Sciences Group, Burlington, MA).

Data Analysis

Off-line analyses were performed using Clampfit software (Molecular Devices). Comparisons between groups were carried out using Students's *t*-test and ANOVA with Bonferroni post hock testing using OriginPro. ANCOVA tests were performed with Prism (Graphpad, La Jolla, CA). Power spectra were compiled from current clamp recordings using ramps. All data were tested for normality using the D'Agostino-Pearson omnibus test and was normally distributed ($P \geq 0.05$). Fluorescence curve areas were calculated for the full record using the integration function in OriginPro. Differences were considered significant at values of $P \leq 0.05$. All results are presented as means ± SE.

Results

Whole cell patch-clamp recordings were conducted on a total of 148 Pf neurons. Calcium transients were recorded in 61 of these neurons while 87 were recorded without calcium dyes. All neurons were localized as previously described [22,47]. Cells were localized immediately anterior or posterior to the *fasciculus retroflexus (fr)* (Fig. 1 A). Cells were mainly spindle-shaped and possessed sparsely branching bipolar dendrites (Fig. 1 B). Cells were recorded regardless of the presence or absence of LTS currents as depolarizing current ramps were applied from membrane potentials known to prevent the activation of these currents, which are known to be activated at much more hyperpolarized membrane potentials [22,23].

Previous work showed no difference in resting membrane potential between Pf cells with LTS and those that lacked LTS [22]. More depolarizing average resting membrane potential values were observed for higher affinity Ca^{2+} dyes (see calibration curves below; OGB1 −44±2mV, $n = 19$; Fura 2 −48±1mV, $n = 25$; Bis Fura −50±2mV $n = 17$), showing significant differences only between OGB1 and Bis Fura (ANOVA, $F_{2, 58} = 5.61$, P=0.006; Fura 2 vs. OGB1, P=0.076; Bis Fura vs. OBG1, P=0.005; Fura 2 vs. Bis Fura, P=0.646), and between dye groups and control cells (CTRL −56.3±0.88mV, $n = 87$; Fura 2 vs. CTRL, $P=2.4\times10^{-8}$; Bis Fura vs. CTRL, $P=5.8\times10^{-4}$, OGB1 vs. CTRL, $P=4.8\times10^{-13}$). We studied the presence of fluorescent calcium oscillations in the cell soma and proximal dendrites in relation to depolarizing current ramps. We further characterized the fluorescent calcium

oscillations with the application of broad as well as specific voltage-dependent calcium channel blockers. Finally, we tested the fluorescent calcium oscillations in the presence and absence of TTX.

Calibration

In order to determine the differential affinity for intracellular calcium concentration [Ca^{2+}] by Fura 2, Bis Fura, and OGB, Kd values for each dye were analyzed using calcium calibration buffers. The calibration curves were averages of 4 calibration experiments performed with Fura and Bis fura and 6 experiments for OGB1 for each [Ca^{2+}] (see supplemental Fig. 1). OGB1 showed the highest affinity with a K_d = 210±10nM, followed by Fura 2 with a K_d = 322±8nM. As expected, Bis Fura had the lowest affinity K_d = 885±6nM. It should be noted, that some non-linearity was present in the calibration curves toward saturating calcium concentrations. If the saturation values are ignored, the K_d for OGB1 and Bis Fura was close to the manufacturer specified values.

Depolarizing ramps generated calcium transients in Pf Neurons

We tested the hypothesis that in the presence of TTX and synaptic blockers, depolarizing current ramps will induce measureable calcium transients. Each patched neuron was depolarized with a current ramp in current clamp mode, which induced calcium oscillations regardless of dye (Fig. 2 A, black records). Frequencies ranged from beta (13–20 Hz) to low gamma (20–40 Hz). Fluorescence traces showed an increase in ΔF/F coinciding with the increase in current (Fig. 2 C, black records). Blocking P/Q-, N-, and T- type calcium channels with the non-specific calcium channel blocker Cd^{2+} completely eliminated calcium oscillations in the electrical recording (Fig. 2, red records) and calcium transients in the fluorescence recording.

The average integrated curve area of fluorescence transients recorded in both the soma (Fura 2 104±14.3, n = 10; Bis Fura 37±11, n = 5; OGB1 124±39 ΔF*msec, n = 6) and proximal dendrite (Fura 2 70±9.2, n = 7; Bis Fura 24±4, n = 5; OGB1 62±15 ΔF*msec, n = 13) decreased significantly for both the soma recordings (Fura 2 32±9.8, P=0.027; Bis Fura 10±8.9, P=0.026; OGB1 7±1.3 ΔF*msec, P=0.032), and dendrite recordings (Fura 2 23±1.3, P=0.001; Bis Fura 8.8±0.7, P=0.034; OGB1 5±0.6 ΔF*msec, P=0.002) using a Student's *t*-test (Fig. 2 D, E). Ratiometric measurements, converted to calcium concentrations using calibration curves, showed resting concentrations of 41±26 nM, somatic (n = 10) and 62±14 nM, dendritic (n = 11) for Fura 2, and 45±20 nM, somatic (n = 6) and 51±23 nM, dendritic (n = 5) for Bis Fura. The calcium transients showed a peak of 137±39, somatic and 90±15, dendritic for Fura 2 and 82±49, somatic and 53±22 dendritic for Bis Fura. Please note that absolute calcium concentrations are tentative since the effects of the unique intracellular environment can widely affect the dye K_d values.

We also examined the fluorescent calcium transients using synaptic blockers only, and omitting TTX. We tested whether the fluorescence curve area decreased when TTX was omitted, causing calcium channels to be inactivated by unclamped nearby synaptic neuronal activity as well as by recurrent over activation of Pf dendritic compartments. While the fluorescence curve area appears slightly smaller when comparing synaptic blockers with and without TTX for each dye (Figs. 3, 4; D, E), the differences were not statistically significant (Fura 2 P=0.866, Bis Fura P=0.096, OGB1 P=0.22). Also, while the cells recorded with synaptic blockers only appeared to have higher oscillation frequencies (Fig. 3 B), the mean peak oscillation frequencies were not statistically different (Fura 2 P=0.25, Bis Fura P=0.154, OGB1 P=0.088). The average integrated curve areas for both the soma (Fura 2 85±17.1, n = 5; Bis Fura 72±13.7, n = 6; OGB1 55±21.7, n = 4) and proximal dendrite (Fura 2 27±3, n = 8; Bis Fura 27±2.6, n = 9; OGB1 12±2.1, n = 15) showed a significant decrease

in fluorescence when Cd^{2+} was bath-applied for both soma (Fura 2 36±5.1, P=0.016; Bis Fura 26±4, P=0.007; OGB1 5±0.6, P=0.0467) and proximal dendrite areas (Fura 2 16±2.7, $P=7.5\times10^{-4}$; Bis Fura 13±0.98, $P=6.3\times10^{-4}$; OGB1 5±0.9, $P=4.4\times10^{-4}$).

Effects of specific calcium channel blockers on Pf fluorescent calcium transients

Our previous work has shown that calcium oscillations in the Pf are due to P/Q- and N-type voltage-dependent calcium channels [22]. We studied the effects of both AgA (a specific P/Q- type calcium channel blocker, 200 μM) and CgTx (a specific N- type calcium channel blocker, 1.5 – 2.5 μM) in order to confirm that P/Q- and N- type calcium channels are responsible for the observed fluorescent calcium transients (n= 19). The combination of AgA and CgTx completely abolished electrical oscillations (Fig. 34 A, B red records) as well as calcium transients (Fig. 3, 4 C, red records). The average integrated fluorescence curve areas for soma (Fura 2 105±14.5, $n = 5$; Bis Fura 83±19.3, $n = 6$; OGB1 77±26.2, $n = 6$) and proximal dendrite (Fura 2 26±12.77.1, $n = 7$; Bis Fura 27±3.5, $n = 9$; OGB1 18±5.4, $n = 13$) showed a significant decrease in both the soma (Fura 2 33±9.8, P=0.027; Bis Fura 31±19.3, P=0.048; OGB1 7±2.9, P=0.047) and proximal dendrite (Fura 2 16±2.4, $P=1.7\times10^{-4}$; Bis Fura 14±2.8, $P=3.4\times10^{-4}$; OGB1 3±0.5, P=0.008).

Calcium oscillations were evident in the calcium-dependent fluorescence signal

We used OGB1 to record calcium transients at higher frame rates in order to test the hypothesis that calcium oscillations recorded in the electrical patch recordings would also be present in fluorescent calcium recordings. We observed simultaneous oscillations in both patch and fluorescent records in 11 OGB1 filled neurons. In Figure 5, the electrical recording is shown in the black record in part A. Fluorescence was recorded from the soma and two proximal dendrite branches (red, pink, and green records). The red somatic fluorescence record shows peaks that match each oscillation peak in the black electrical record, although the fluorescence peaks had a slight delay in comparison to the electrical peaks (Fig. 5 B, ~10 msec delay initially and decreased with each successive oscillation). The dendrite records (pink and green records) show oscillations that matched the electrical record. Some oscillation peaks can be seen on dendrite 1, but not on dendrite 2 and vice versa. Some oscillation peaks were present in both dendrite records while others present in the dendrite records may not be evident in the electrical record. It must be noted that the electrical record is from the soma and represents a sum of all activity in the cell, in particular a sum of calcium activity in all of the dendrites. Cross-correlation analysis of the electrical and somatic fluorescence records (Fig. 5 C) indicated a 12 msec lag with a frequency of approximately 15 Hz. This is also supported by the power spectrum (Fig. 5 C), with the somatic fluorescence signal showing a broad peak centered at 14 Hz (red line) which matches the 15 Hz peak in the electrical record (black line).

The full calcium transient showed a graded response (Fig. 6B) as the fluorescence signal was measured sequentially across 50 μm of proximal dendrite in 5 μm steps (Fig. 6A). Oscillations were conserved along the length of the dendrite with few gaps. The calcium flux dropped rapidly in the first 30μm of dendrite but began to level off after (Fig. 6C).

Characterization of oscillation frequency and age dependence

The peak oscillation frequency was plotted against age of each fluorescent cell (Fig. 7 C). Linear regression was performed on each dye group. While Fura 2 and Bis Fura labeled cells decreased in oscillation frequency with age, OGB1 cells increased in oscillation frequency with age. ANCOVA analysis showed that none of these trend lines were significantly different. An age/frequency plot of the control cells (which lacked any calcium dye) showed an increase in frequency as age increased (Fig. 7 A). This is in agreement with our previously published results showing that, early in Pf development, the maximum oscillatory

frequency is in the alpha and beta ranges and gradually increases and plateaus in the gamma range with age [22].

Cells were divided into two age groups; 9 – 14 days old (DO) and 15 – 19 days old (Fig. 7B). The mean peak frequency of oscillations in Fura 2 filled cells in the two age groups were compared (9 – −14 DO 19±1.4 Hz, $n = 16$; 15 – 19 DO 15±0.94 Hz, $n = 9$) and were not significantly different (P=0.059). Bis Fura filled cells were not compared due to too few cells in the 15 – 19 DO age group. OGB1 filled cells (9 −14 DO 21±1.7 Hz, $n = 12$; 15 – 19 DO 19±3.7 Hz, $n = 7$) displayed no significant difference between groups (P=0.583). Control cells (9 −14 DO 34±2.1 Hz, $n = 53$; 15 – 19 DO 49±2 Hz, $n = 34$) displayed a significant difference between age groups ($P=1.4\times10^{-5}$).

The mean peak frequency of dye filled cells in each age group was compared to control cells (Fig. 7 D). The Fura 2 and OGB1 peak frequencies in the 9 – 14 DO age group were significantly lower than the control frequency (Fura 2 vs. CTRL, $P=1.9\times10^{-4}$; OGB1 vs. CTRL, $P=3.4x10^{-6}$). Both Fura 2 and OGB1 peak frequencies were significantly lower than the control frequency in the 15 – 19 DO age group (Fura 2 vs. CTRL, $P=1\times10^{-8}$; OGB1 vs. CTRL, P=0.003). This indicates that all of the calcium dyes decreased oscillation frequencies, possibly due to the calcium buffering effects of the dye. Averaged power spectra for each group are provided in supplemental figure 2. We should note that TTX decreased oscillation amplitude. This has been observed in our previous studies and was attributed to the lack of high frequency action potentials and the associated decrease in synaptic activity.

Discussion

The present study generated the following important original findings. 1) Ratiometric analyses using two separate calcium dyes revealed that calcium concentrations increased in Pf dendrites in parallel with the electrical signal from the patch electrode. 2) Fast imaging using a third dye showed that the peaks in calcium flux paralleled the oscillations in the electrical signal, although probably buffering of calcium by the dye reduced the frequency of the oscillations. 3) The mechanism behind both the imaged calcium oscillations and the parallel ramp-induced electrical oscillations was due to high threshold, voltage-dependent P/Q-type and N-type calcium channels. In this study, we found that Pf neurons produced measureable calcium transients in response to depolarizing current ramps even though all APs and synaptic inputs were blocked. Beta/gamma oscillations present in the recorded electrical activity were also present in the fluorescent calcium activity signal, and these oscillations were evident in both the soma and proximal dendrites. This is the first time that ramp-induced calcium oscillations have been described in the Pf using calcium sensitive dyes. These oscillations have been reported previously in cortical, thalamic, hippocampal, and cerebellar cells. The advantage of visualizing these oscillations using dyes rather than only patch clamp recordings is that spatial differences can be detected, whereas patch clamp recordings only show average oscillatory activity for the entire cell. These experiments used a variety of dyes in order to determine which work best for analyzing calcium oscillations. We focused on Fura, Bis Fura, and OGB1 because they presented the best results. We focused on using Fura and Bis Fura to provide the easiest and most accurate analysis of calcium concentrations due to their ratiometric properties. Both Fura and Bis Fura were used due to possibility that the higher affinity Fura would low-pass filter observed calcium dynamics. These dyes showed a moderate increase in calcium concentration in the dendrites with the peak of the calcium transient. OGB1 was used because it was best at visualizing the calcium oscillations with higher acquisition rates than those used for ratiometric analysis. This dye showed that, while individual oscillations could be visualized by the rapid imaging, the frequency of the oscillations was reduced, perhaps due to its [Ca^{2+}] buffering capacity.

The mechanism behind the generation of these oscillations has been shown to involve high-threshold voltage-dependent P/Q- and N- type calcium channels [22,23]. Herein we replicated our previous results using electrical recordings, showed that oscillations present in calcium fluorescence signals matched the oscillations in membrane potential signals, and the use of AgA and CgTx allowed us to eliminate both electrical oscillations and fluorescent calcium transients in Pf neurons.

Our resting somatic calcium concentrations were similar to resting concentrations reported in thalamic neurons [2, 4]. If we examine calcium concentrations in the dendrites, we find slightly lower resting calcium concentrations, but still within range in comparison to dendritic calcium concentrations reported in hippocampal neurons and cortical neurons (45–133 nM) [3, 11, 38]. In addition, intracellular dye concentrations achieved in this study were capable of significantly changing resting membrane potential, according to their affinity to [Ca^{2+}]. These novel results suggest the involvement of a Ca^{2+}-dependent potassium current in the maintenance of resting membrane potential of Pf neurons. Other work has shown that small-conductance type K+ channels activate in conjunction with Ca2+ influx through T-type calcium channels in thalamic reticular neurons [5]. This study did not control extraneous potassium currents thus it is possible for uncontrolled calcium mediated potassium channel activation to alter the membrane potential, which would explain the changes in resting membrane potential levels described here. This may include other potassium channels such as BK type potassium channels.

We show a moderate increase in calcium concentration in the dendrites with the peak of the calcium transient. The peak calcium concentration was lower than calcium concentrations seen in the dendrites of cortical neurons during firing (383 nM) [3]. This was probably due to the lack of firing in Pf neurons using synaptic blockers and TTX. More specifically, we were recording oscillatory activity, thus the calcium transients would be expected to be of lower amplitude. It is possible that the depolarizing current ramps did not elicit the maximum possible amplitude calcium transients. Also, caution must be used when interpreting absolute calcium concentrations since the K_d value for each dye can vary widely depending on intracellular conditions such as temperature, ionic strength, and pH.

Early descriptions of the RAS suggested that it participates in “tonic” or continuous arousal [30]. Lesions of this region eliminated tonic arousal [46], and it is possible that PPN input to the Pf helps to maintain such activity. Using OGB1, we were able to conduct high-speed calcium dye recordings, showing calcium oscillations in Pf neurons. The oscillations present in the somatic fluorescence records closely matched the electrical patch clamp recordings, which indicated a summation of calcium signals arriving from the dendrites. The frequency and cross-correlation data in turn support the contention that the oscillations seen in the calcium signal were the same frequency as those observed in the patch clamp record. Some time delays were seen in the somatic fluorescence records, which may have been due to the larger cytosolic volume of the soma and kinetics of the dyes. We also observed calcium oscillations in the proximal dendritic fluorescence recordings. Interestingly, these oscillations may not exactly match oscillations evident in the patch clamp recordings or the somatic fluorescence recordings. Some oscillation peaks may be missing or may be present in some dendrites, but not others. Also, some peaks may exactly match the patch clamp recording while others may be slightly out of phase. This may be indicative of dendritic subdomains with some dendrites having greater influence over the total calcium signal. Separate dendrites or regions within a single dendrite may oscillate at slightly different phases, while all of the separate oscillatory dendritic potentials are integrated in the recording at the soma. We know that these oscillations are dendritic in origin due to the high depolarizing voltage, as previously described [33]. While we were not able to visualize distal dendrites and determine the precise origin of each component of the full oscillatory

signal, we can see that different dendrites provide parts of the total signal and that some dendrites may provide more than others.

Evoked calcium transients in Pf neurons showed a distance-dependent incremental scaling with increments up to 50 μm. While the back propagation of calcium transients decreased with distance from the soma, it is still possible that large calcium accumulations may occur at distal sites. This is similar to oscillations observed in “specific” TC relay neurons. P/Q-type voltage-dependent calcium channels are found throughout the brain [16, 26]. More specifically these channels are found on the dendrites of the bushy TC cells. The increase in calcium has been visualized in the dendrites of these relay neurons using calcium imaging [33]. While we cannot determine the actual membrane potential of the dendrites without actually clamping them (voltage clamp of small dendrites leads to rapid dialysis of the intracellular domain), the membrane potential is probably lower than the ones seen at the somatic level during patch recordings. This is due to total membrane capacitance between the electrode and the dendritic compartments. Unfortunately, we were unable to visualize very distal compartments using calcium dyes in Pf neurons due to their sparse, thin dendrites. Very low dye concentrations in these distal dendritic compartments, coupled with the presence of few dendrites, prevented us from obtaining recordings with adequate signal-to-noise ratios. While we were unable to visualize the distal compartments in Pf neurons, it may be possible to visualize distal compartments in neurons with more compact morphology such as PPN neurons.

Oscillations in the proximal dendrites appeared to be continuous across sequential sampling regions. We originally expected to see localized regions of fluorescence with oscillations, indicating specific regions of calcium channels. The continuous presence of fluorescent oscillations suggests the continuous presence of calcium channels across the proximal dendrites. While this is possible, we must note that the intrinsic calcium buffering capabilities of calcium indicators can accelerate the spatial spread of calcium signals. Typically, calcium diffusion is spatially limited due to binding to large endogenous calcium binding proteins. Conversely, calcium buffers such as indicator dyes are relatively small, highly mobile molecules that bypass calcium binding proteins and allow unbinding at more distal locations [15]. Further experiments will need to be conducted to analyze the spatial distribution of voltage-dependent calcium channels across dendritic sub-domains, possibly using higher molecular weight dextran-conjugated calcium indicators. Bulk loading AM-ester versions of each dye may also be a viable alternative for studying dendritic sub-domains as well as providing better distal labeling with lower dye concentrations.

The separate age groups of our control data showed that oscillatory activity plateaued in the gamma band range in older animals (15–19 days old), matching earlier studies [22, 23]. It should also be noted that this is the period when the largest developmental decrease in REM sleep begins to level off at the adult REM sleep levels [21]. Using the same comparison with the calcium dye groups, we did not see the same developmental increase in frequency. The presence of the calcium dye appeared to greatly vary the oscillation frequency and thus confound efforts to study frequency related results. Our results show that the presence of calcium dyes decreased the peak oscillation frequency in both young and old animals in comparison to control data. This is probably due to the dye acting as a calcium buffer as well as slowing calcium kinetics [15, 38]. While the oscillation frequency may be slower, this, however, does not prevent us from studying frequency data. We should still be able observe relative changes in oscillation frequency in response to drugs or other stimuli. Caution will be necessary in interpreting any frequency data and much larger experimental groups will be necessary to fully elucidate questions regarding frequency effects.

Recently, new treatments for movement disorders such as Parkinson's disease (PD) have centered on using deep brain stimulation (DBS) in the centromedian-parafascicular (CM/Pf) complex of the thalamus [19]. Rodents possess mostly Pf rather than the CM nucleus. While neurodegeneration of this complex has been reported in PD patients [13], animal models have shown extensive alterations in CM/Pf activity [1, 9, 31, 32]. Moreover, strong antiparkinsonian benefits have been obtained by applying high-frequency stimulation of the Pf nucleus in rodents [19]. In this study, we showed that calcium oscillations can be studied visually in the Pf nucleus at the single cell level and confirmed that specific calcium channels play a significant role in their generation. The importance of this oscillatory activity may be considerable since Pf neurons send widespread projections throughout the brain. Thus, it is possible that novel pharmacological treatments can be developed to target oscillatory output of the Pf nucleus for treatment of certain movement disorders, rather than the use of electrical stimulation of the CM/Pf complex.

The present findings present a viable methodology for studying high-speed oscillations without the use of multi-photon imaging systems. The advantage of using a wide field based imaging system is that we can simultaneously record from many areas without having to account for timing delays due to laser seek time. Wide field imaging is particularly well suited for visualizing oscillations since all imaging data must be acquired in a single run without averaging (oscillations are almost never in phase from ramp to ramp). Granted, wide field imaging has its limitations, in particular, lower signal-to-noise ratio and potential signal "bleed" from one area of interest to the next. Also, the presence of high calcium dye concentrations modulates the spatiotemporal characteristics limiting the variety of experiments possible with this technique. This mainly means careful analysis is necessary in interpreting results from these experiments. Some of these problems can be resolved with a multi-photon microscope, visualizing distal dendrites in particular. Unfortunately, the cost and availability of multi-photon microscopes are still limiting factors while wide-field imaging systems have greater availability. We used a combination of dyes in order to best elucidate the various properties of sub threshold oscillations. While fewer dyes may be used, we wanted to provide a broader basis for researchers in the community to relate these techniques to their experiments. We suggest that oscillatory activity generated in the Pf may help stabilize coherence related to arousal and relay this activation to the cortex, thus providing a stable activation state during waking. Much work is necessary to support this speculation, but calcium imaging techniques and localized calcium data such as those we describe provide a useful stepping-stone in such investigations, especially since intracellular Ca^{2+} ions are known to act as key second-messengers of intracellular pathways.

Supplementary Material

Refer to Web version on PubMed Central for supplementary material.

Acknowledgments

The authors would like to thank Dr. Abdallah Hayar for his assistance with calcium signal analysis. This work was supported by USPHS award R01 NS020246, and by core facilities of the Center for Translational Neuroscience supported by P20 GM104325 (to EGR) and UL1 TR000039. In addition, Dr. Urbano was supported by FONCyT, Agencia Nacional de Promoción Científica y Tecnológica (http://www.ifibyne.fcen.uba.ar/new/): BID 1728 OC.AR. PICT 2008–2019.

References

1. Aymerich MS, Barroso-Chinea P, Perez-Manso M, Munoz-Patino AM, Moreno-Igoa M, Gonzalez-Hernandez T, Lanciego JL. Consequences of unilateral nigrostriatal denervation on the thalamostriatal pathway in rats. Eur J Neurosci. 2006; 23:2099–108. [PubMed: 16630057]

2. Budde T, Sieg F, Braunewell KH, Gundelfinger ED, Pape HC. Ca2+-induced Ca2+ release supports the relay mode of activity in thalamocortical cells. Neuron. 2000; 26:483–92. [PubMed: 10839366]
3. Cornelisse LN, van Elburg RA, Meredith RM, Yuste R, Mansvelder HD. High speed two-photon imaging of calcium dynamics in dendritic spines: consequences for spine calcium kinetics and buffer capacity. PLoS One. 2007; 2:e1073. [PubMed: 17957255]
4. Coulon P, Herr D, Kanyshkova T, Meuth P, Budde T, Pape HC. Burst discharges in neurons of the thalamic reticular nucleus are shaped by calcium-induced calcium release. Cell Calcium. 2009; 46:333–46. [PubMed: 19913909]
5. Cueni L, Canepari M, Lujan R, Emmenegger Y, Watanabe M, Bond CT, Franken P, Adelman JP, Luthi A. T-type Ca2+ channels, SK2 channels and SERCAs gate sleep-related oscillations in thalamic dendrites. Nat Neurosci. 2008; 11:683–92. [PubMed: 18488023]
6. Deschenes M, Bourassa J, Doan VD, Parent A. A single-cell study of the axonal projections arising from the posterior intralaminar thalamic nuclei in the rat. Eur J Neurosci. 1996; 8:343–343.
7. Deschenes M, Bourassa J, Parent A. Striatal and cortical projections of single neurons from the central lateral thalamic nucleus in the rat. Neuroscience. 1996; 72:679–687. [PubMed: 9157314]
8. Eckhorn R, Bauer R, Jordan W, Brosch M, Kruse W, Munk M, Reitboeck HJ. Coherent oscillations: a mechanism of feature linking in the visual cortex? Multiple electrode and correlation analyses in the cat. Biol Cybern. 1988; 60:121–130. [PubMed: 3228555]
9. Freyaldenhoven TE, Ali SF, Schmued LC. Systemic administration of MPTP induces thalamic neuronal degeneration in mice. Brain Res. 1997; 759:9–17. [PubMed: 9219857]
10. Garcia-Rill E, Kezunovic N, Hyde J, Simon C, Beck P, Urbano FJ. Coherence and frequency in the reticular activating system (RAS). Sleep Med Rev. 2013 In press.
11. Goldberg JH, Tamas G, Aronov D, Yuste R. Calcium microdomains in aspiny dendrites. Neuron. 2003; 40:807–821. [PubMed: 14622584]
12. Gray CM, Singer W. Stimulus-specific neuronal oscillations in orientation columns of cat visual cortex. Proc Natl Acad Sci USA. 1989; 86:1698–702. [PubMed: 2922407]
13. Henderson JM, Carpenter K, Cartwright H, Halliday GM. Loss of thalamic intralaminar nuclei in progressive supranuclear palsy and Parkinson's disease: clinical and therapeutic implications. Brain. 2000; 123(Pt 7):1410–1421. [PubMed: 10869053]
14. Herrero MT, Barcia C, Navarro JM. Functional anatomy of thalamus and basal ganglia. Childs Nerv Syst. 2002; 18:386–404. [PubMed: 12192499]
15. Higley MJ, Sabatini BL. Calcium signaling in dendritic spines. Cold Spring Harb Perspect Biol. 2012; 4:a005686. [PubMed: 22338091]
16. Hillman D, Chen S, Aung TT, Cherksey B, Sugimori M, Llinas RR. Localization of Ptype calcium channels in the central nervous system. Proc Natl Acad Sci U S A. 1991; 88:7076–7080. [PubMed: 1651493]
17. Iannuccelli E, Mompart F, Gellin J, Lahbib-Mansais Y, Yerle M, Boudier T. NEMO: a tool for analyzing gene and chromosome territory distributions from 3D-FISH experiments. Bioinformatics. 2010; 26:696–697. [PubMed: 20080510]
18. Jeon D, Kim C, Yang YM, Rhim H, Yim E, Oh U, Shin HS. Impaired long-term memory and long-term potentiation in N-type Ca2+ channel-deficient mice. Genes Brain Behav. 2007; 6:375–388. [PubMed: 16939638]
19. Jouve L, Salin P, Melon C, Kerkerian-Le Goff L. Deep brain stimulation of the center median-parafascicular complex of the thalamus has efficient anti-parkinsonian action associated with widespread cellular responses in the basal ganglia network in a rat model of Parkinson's disease. J Neurosci. 2010; 30:9919–9928. [PubMed: 20660274]
20. Jouvet-Mounier D, Astic L, Lacote D. Ontogenesis of the states of sleep in rat, cat, and guinea pig during the first postnatal month. Dev Psychobiol. 1970; 2:216–239. [PubMed: 5527153]
21. Kao JP. Practical aspects of measuring [Ca2+] with fluorescent indicators. Methods Cell Biol. 1994; 40:155–181. [PubMed: 8201975]
22. Kezunovic N, Hyde J, Simon C, Urbano FJ, Williams DK, Garcia-Rill E. Gamma band activity in the developing parafascicular nucleus. J Neurophysiol. 2012; 107:772–784. [PubMed: 22090455]

23. Kezunovic N, Urbano FJ, Simon C, Hyde J, Smith K, Garcia-Rill E. Mechanism behind gamma band activity in the pedunculopontine nucleus. Eur J Neurosci. 2011; 34:404–415. [PubMed: 21722210]
24. Llinas RR, Choi S, Urbano FJ, Shin HS. Gamma-band deficiency and abnormal thalamocortical activity in P/Q-type channel mutant mice. Proc Natl Acad Sci U S A. 2007; 104:17819–24. [PubMed: 17968008]
24. Llinás RR, Grace AA, Yarom Y. In vitro neurons in mammalian cortical layer 4 exhibit intrinsic oscillatory activity in the 10- to 50-Hz frequency range. Proc Natl Acad Sci USA. 1991; 88:901–901.
26. Llinas RR, Steriade M. Bursting of thalamic neurons and states of vigilance. J Neurophysiol. 2006; 95:3297–3308. [PubMed: 16554502]
27. Luo M, Perkel DJ. Long-range GABAergic projection in a circuit essential for vocal learning. J Comp Neurol. 1999; 403:68–84. [PubMed: 10075444]
28. Minamimoto T, Kimura M. Participation of the thalamic CM-Pf complex in attentional orienting. J Neurophysiol. 2002; 87:3090–3101. [PubMed: 12037210]
29. Miura K RJ. Bleach Corrector EMBL Heidelberg. 2010
30. Moruzzi G, Magoun HW. Brain stem reticular formation and activation of the EEG. Electroencephalogr Clin Neurophysiol. 1949; 1:455–473. [PubMed: 18421835]
31. Orieux G, Francois C, Feger J, Yelnik J, Vila M, Ruberg M, Agid Y, Hirsch EC. Metabolic activity of excitatory parafascicular and pedunculopontine inputs to the subthalamic nucleus in a rat model of Parkinson's disease. Neuroscience. 2000; 97:79–88. [PubMed: 10771341]
32. Parr-Brownlie LC, Poloskey SL, Bergstrom DA, Walters JR. Parafascicular thalamic nucleus activity in a rat model of Parkinson's disease. Exp Neurol. 2009; 217:269–281. [PubMed: 19268664]
33. Pedroarena C, Llinas R. Dendritic calcium conductances generate high-frequency oscillation in thalamocortical neurons. Proc Natl Acad Sci U S A. 1997; 94:724–728. [PubMed: 9012852]
34. Raeva SN. The role of the parafascicular complex (CM-Pf) of the human thalamus in the neuronal mechanisms of selective attention. Neurosci Behav Physiol. 2006; 36:287–95. [PubMed: 16465496]
35. Rasband, W. (1997–2004), ImageJNational Institutes of Health, , Bethesda, Maryland, USA.
36. Rhodes PA, Llinas R. A model of thalamocortical relay cells. J Physiol. 2005; 565:765–781. [PubMed: 15613378]
37. Sabatini BL, Oertner TG, Svoboda K. The life cycle of Ca(2+) ions in dendritic spines. Neuron. 2002; 33:439–452. [PubMed: 11832230]
38. Segal M. Imaging of calcium variations in living dendritic spines of cultured rat hippocampal neurons. J Physiol. 1995; 486(Pt 2):283–295. [PubMed: 7473196]
39. Simon C, Kezunovic N, Williams DK, Urbano FJ, Garcia-Rill E. Cholinergic and glutamatergic agonists induce gamma frequency activity in dorsal subcoeruleus nucleus neurons. Am J Physiol Cell Physiol. 2011; 301:C327–C335. [PubMed: 21543743]
40. Steriade M. Unspecific systems of inhibition and facilitation of potentials evoked by intermittent light. J Neurophysiol. 1960; 23:602–617.
41. Takahashi A, Camacho P, Lechleiter JD, Herman B. Measurement of intracellular calcium. Physiol Rev. 1999; 79:1089–1125. [PubMed: 10508230]
42. Thevenaz P, Ruttimann UE, Unser M. A pyramid approach to subpixel registration based on intensity. IEEE Trans Image Process. 1998; 7:27–41. [PubMed: 18267377]
43. Uchitel OD, Protti DA, Sanchez V, Cherksey BD, Sugimori M, Llinas R. P-type voltage-dependent calcium channel mediates presynaptic calcium influx and transmitter release in mammalian synapses. Proc Natl Acad Sci U S A. 1992; 89:3330–3333. [PubMed: 1348859]
44. Urbano FJ, Kezunovic N, Hyde J, Simon C, Beck P, Garcia-Rill E. Gamma band activity in the reticular activating system. Front Neurol. 2012; 3:6. [PubMed: 22319508]
45. Van der Werf YD, Witter MP, Groenewegen HJ. The intralaminar and midline nuclei of the thalamus. Anatomical and functional evidence for participation in processes of arousal and awareness. Brain Res Brain Res Rev. 2002; 39:107–140. [PubMed: 12423763]

46. Watson RT, Heilman KM, Miller BD, King FA. Neglect after mesencephalic reticular formation lesions. Neurology. 1974; 24:294–298. [PubMed: 4205158]

47. Ye M, Hayar A, Garcia-Rill E. Cholinergic responses and intrinsic membrane properties of developing thalamic parafascicular neurons. J Neurophysiol. 2009; 102:774–785. [PubMed: 19474169]

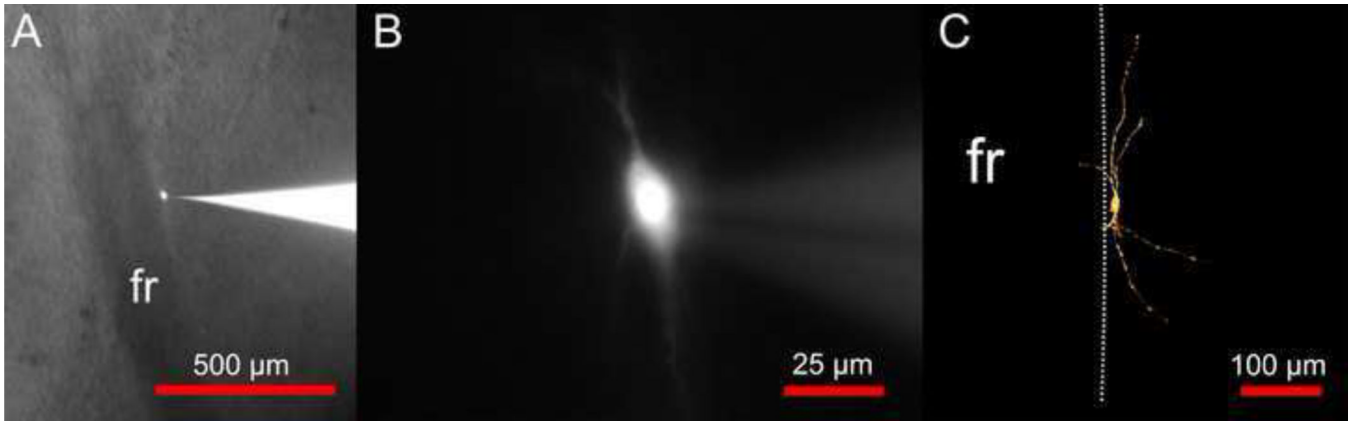

Fig. 1.

Localization and morphology of Pf neurons. A. Location of a single recorded neuron immediately posterior to the fasciculus retroflexus (fr) in a parasagittal thalamic section (bright field). B. Wide field fluorescence image of the same neuron identified with intracellular injection of Alexa Fluor 594. Note the sparsely branching processes. C. Maximum projection confocal image of an Alexa Fluor 594 filled neuron. Long, sparsely branching processes are present

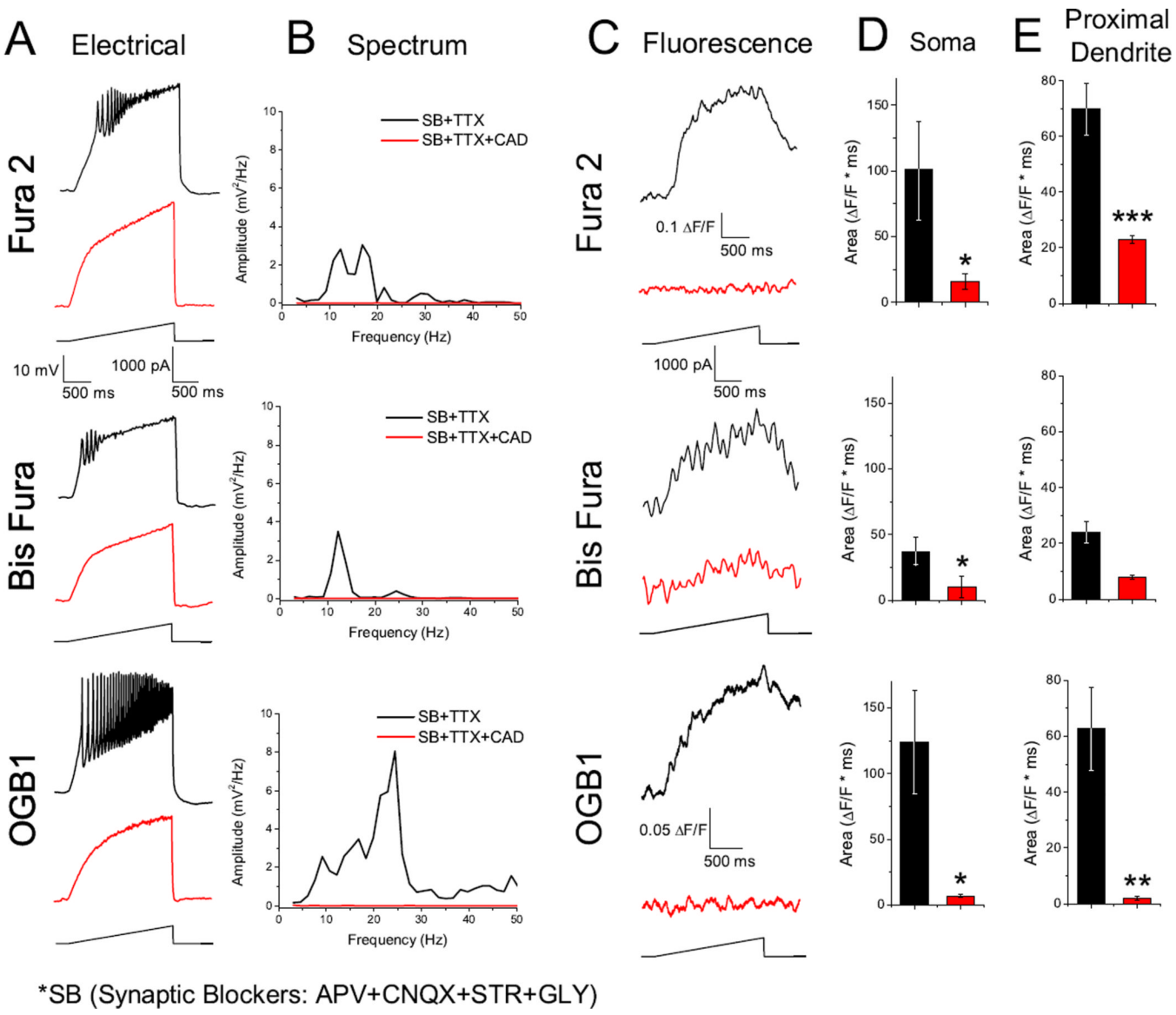

Fig. 2.

Depolarizing current ramps generated oscillations and measureable intracellular calcium transients. A. Representative oscillations of a Pf neuron (black recording) and in the presence of $CdCl_2$ (100 μM; CAD; red recordings) obtained during 2 sec long ramps. B. Overlapping recordings comparing power spectrum amplitudes for oscillations present in A, before and after CAD. C. Somatic fluorescent transients induced by the current ramp (black record), recorded simultaneously with the oscillations present in A. Note how both membrane oscillations and intracellular calcium fluorescence signals were eliminated after CAD (red record). D. Bar graph showing the average integrated somatic curve area for the fluorescence curves before CAD (black bar: Fura 2 104±14.3; Bis Fura 37±11; OGB1 124±39 ΔF*msec) and after CAD (red bar: Fura 2 32±9.8; Bis Fura 10±8.9; OGB1 7±1.3 ΔF*msec). E. Bar graph showing the average integrated proximal dendritic curve area for the fluorescence curves before CAD (black bar: Fura 2 70±9.2; Bis Fura 24±4; OGB1 62±15 ΔF*msec) and after CAD (red bar: Fura 2 23±1.3; Bis Fura 8.8±0.7; OGB1 5±0.6 ΔF*msec). *P< 0.05; **P< 0.01; ***P< 0.001

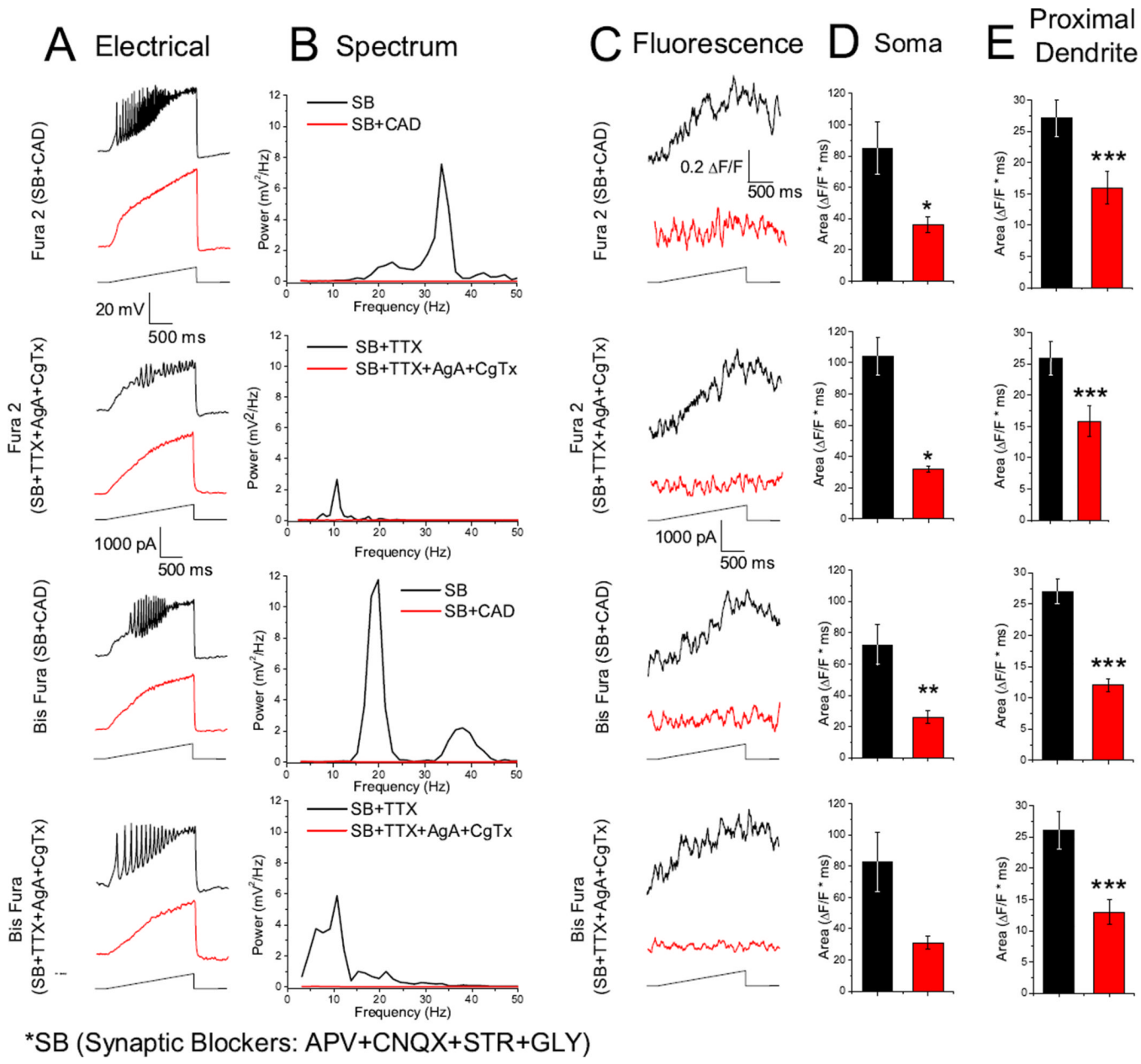

Fig. 3.

N- and P/Q- type calcium channels mediate calcium oscillations in the Pf visualized with Fura 2 and Bis Fura. SB (synaptic blockers). A. Representative calcium oscillations with and without TTX (black record) and after bath application of specific calcium channel blockers AgA and CgTx or the nonspecific calcium channel blocker CAD (red record). Note that calcium oscillations were eliminated by AgA and CgTx, indicating fluorescence (C) was mediated by N- and P/Q- type calcium channels. B. Power spectrum of records shown in A. C. Somatic fluorescence signals recorded simultaneously with oscillations in A. D. Bar graph showing the average integrated somatic curve area for the fluorescence curves before AgA and CgTx (black bar: Fura 2 105±14.5; Bis Fura 83±19.3 ΔF*msec) and after AgA and CgTx (red bar: Fura 2 33±9.8; Bis Fura 31±19.3 ΔF*msec). Synaptic blocker only conditions before CAD (black bar: Fura 2 85±17.1; Bis Fura 72.3±13.8 ΔF*msec) and after CAD (red bar: Fura 2 36.4±5.1; Bis Fura 26±4 ΔF*msec). E. Bar graph showing the average

integrated proximal dendritic curve area for the fluorescence curves before AgA and CgTx (black bar: Fura 2 26±12.77.1; Bis Fura 27±3.5 ΔF*msec) and after AgA and CgTx (red bar: Fura 2 16±2.4; Bis Fura 14±2.8 ΔF*msec). Synaptic blocker only conditions before CAD (black bar: Fura 2 27.1±3; Bis Fura 27±2.7 ΔF*msec) and after CAD (red bar: Fura 2 16±2.7; Bis Fura 12.9±0.98 ΔF*msec) *P< 0.05; **P< 0.01; ***P< 0.001

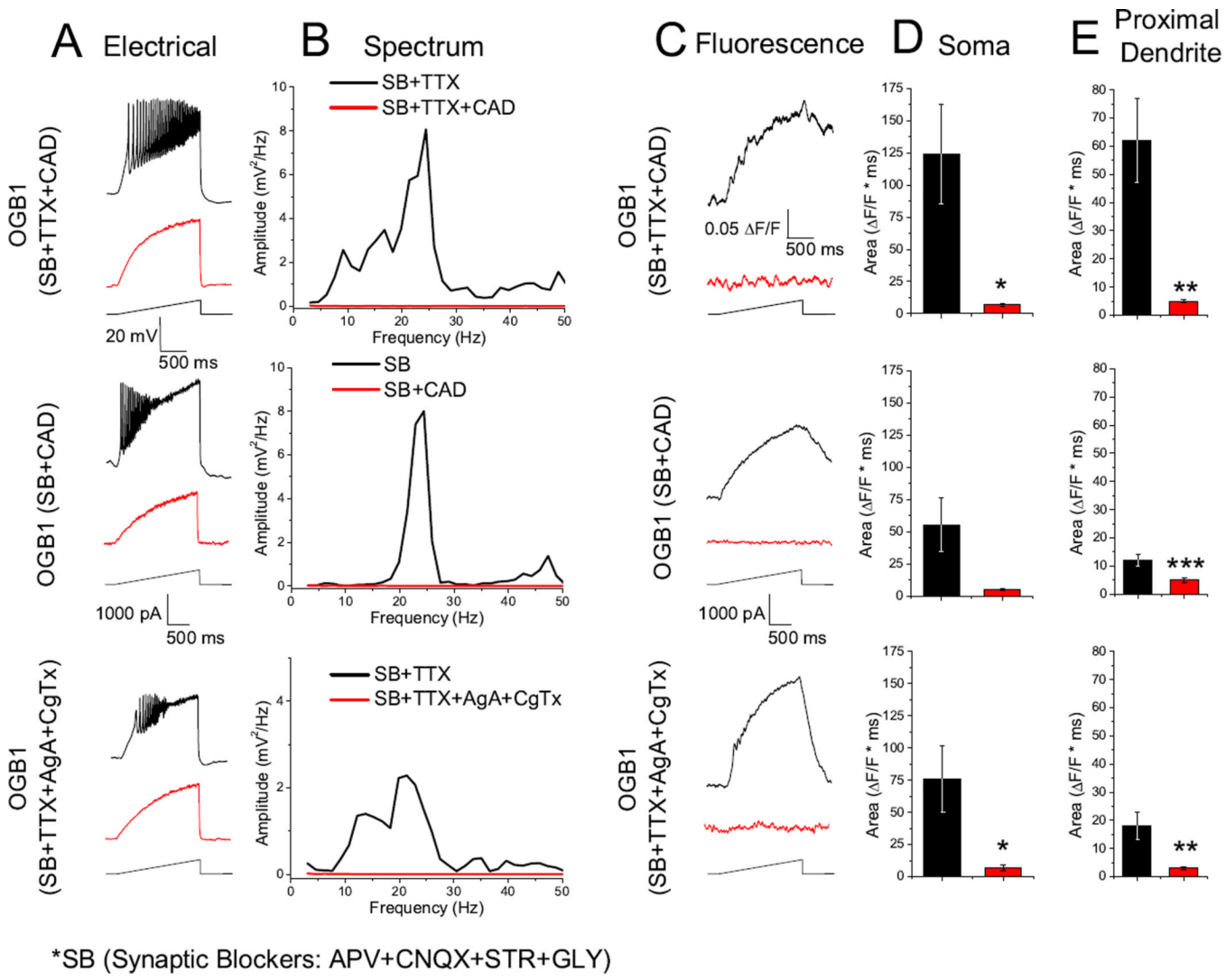

Fig. 4.

N- and P/Q- type calcium channels mediate calcium oscillations in the Pf visualized with OGB1. A. Patch clamp recorded calcium oscillations before (black record) and after (red record) specific and nonspecific calcium channel blockers. B. Power spectra of records in A. C. Fluorescence recordings acquired simultaneously with electrical recordings in A, with (red record) and without (black record) calcium channel blockers. D. Bar graph showing the average integrated somatic curve area for the fluorescence curves before CAD (black bar: SB only 55.5±21.6; with TTX 124±39 ΔF*msec) and after CAD (red bar: SB only 5.5±0.65; with TTX 7±1.3 ΔF*msec). Before AgA and CgTx (black bar: 77±26.2 ΔF*msec) and after (red bar: 7±2.9 ΔF*msec). E. Bar graph showing the average integrated proximal dendritic curve area for the fluorescence curves before CAD (black bar: SB only 12.5±2.1; with TTX 62±15 ΔF*msec) and after CAD (red bar: SB only 5±0.94; with TTX 5±0.6 ΔF*msec). Before AgA and CgTx (black bar: 18±5.4 ΔF*msec) and after (red bar: 3±0.5 ΔF*msec)

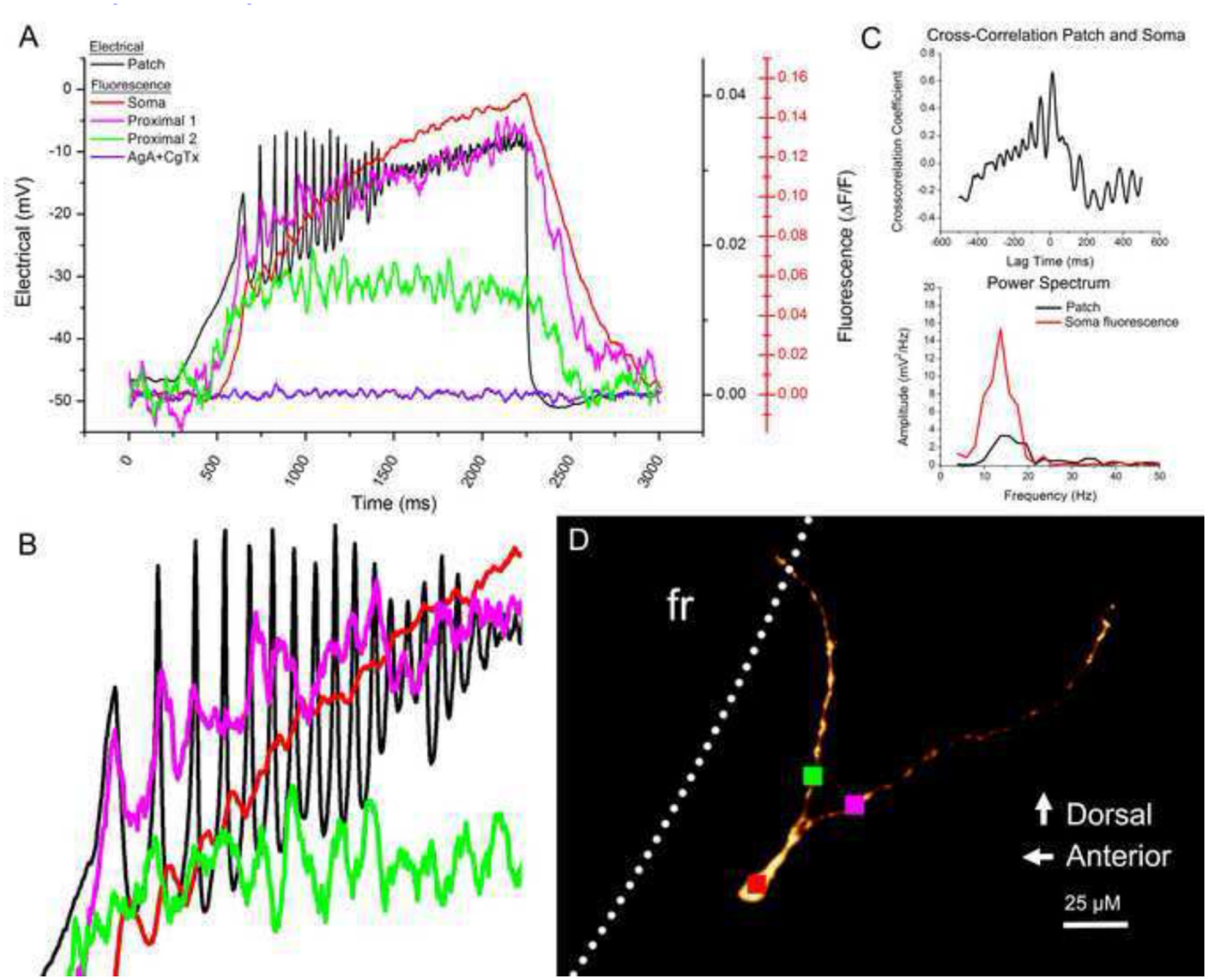

Fig. 5.

Oscillations present in the electrical patch-recorded signal were also evident in the recorded calcium signal. A. Overlay of the electrical patch signal (black record) with the somatic calcium signal (red record) and calcium recordings from two dendritic branches (pink and green, sampling locations shown in D). The somatic calcium signal after AgA and CgTx application is shown in red. Note that the somatic calcium signal uses a different y-axis scaling (red). B. Zoom of the oscillation signal in A. A slight time delay (~10msec and decreasing) is present in the somatic signal. Some oscillations were present in dendritic signals that matched the electrical signal while others were slightly out of phase. C. Cross-correlation graph and power spectra of the patch recording (black) and the somatic fluorescence recording (red). D. Confocal image of the recorded cell indicating fluorescence sampling locations (red, pink and green squares)

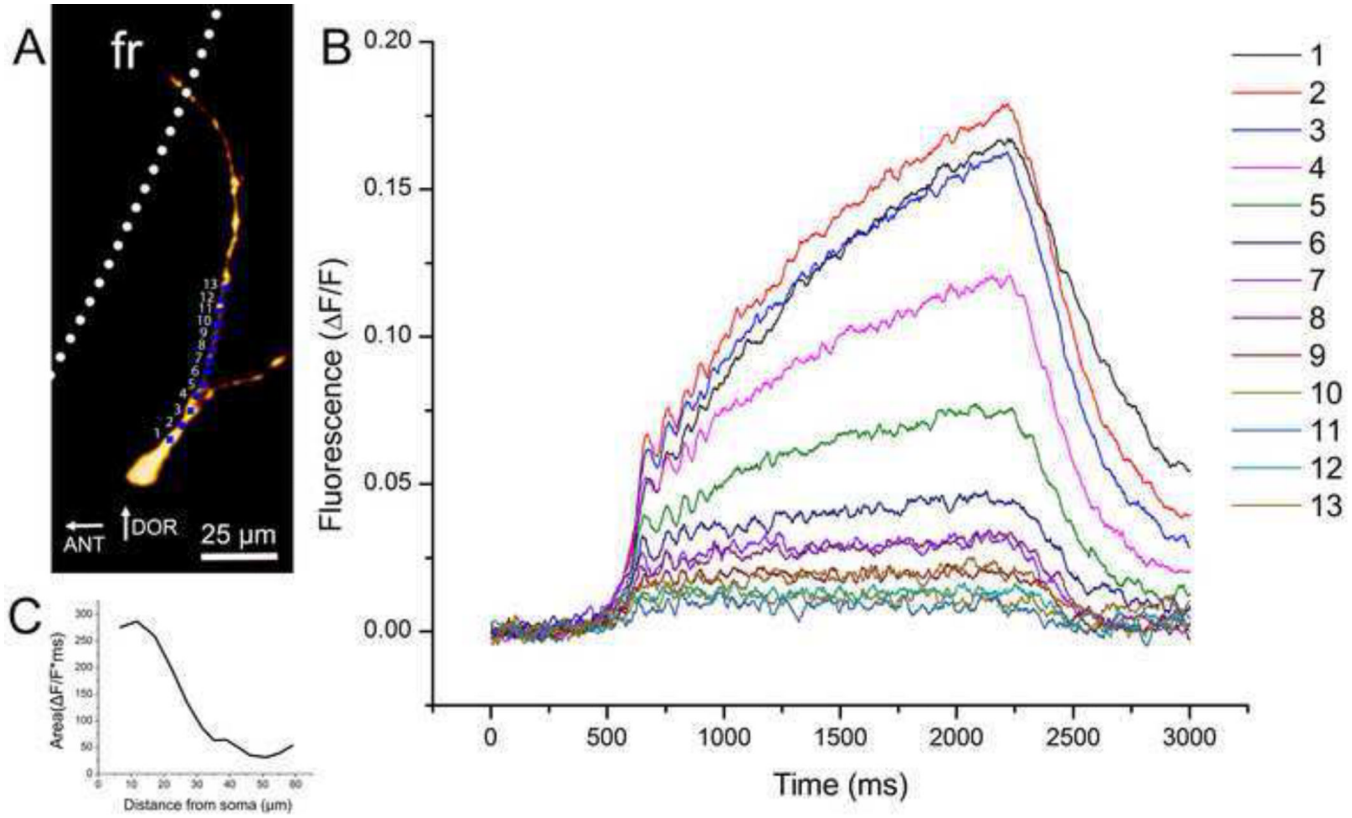

Fig. 6.

Oscillations measured simultaneously in a single dendrite. A. Recording locations for each record in B. B. Graded responses are shown in the calcium signal as it was measured simultaneously across 50 µM of proximal dendrite. Oscillations were evident along the dendrite with few gaps. C. Graph showing the fluorescent trace area in relation to distance from the soma

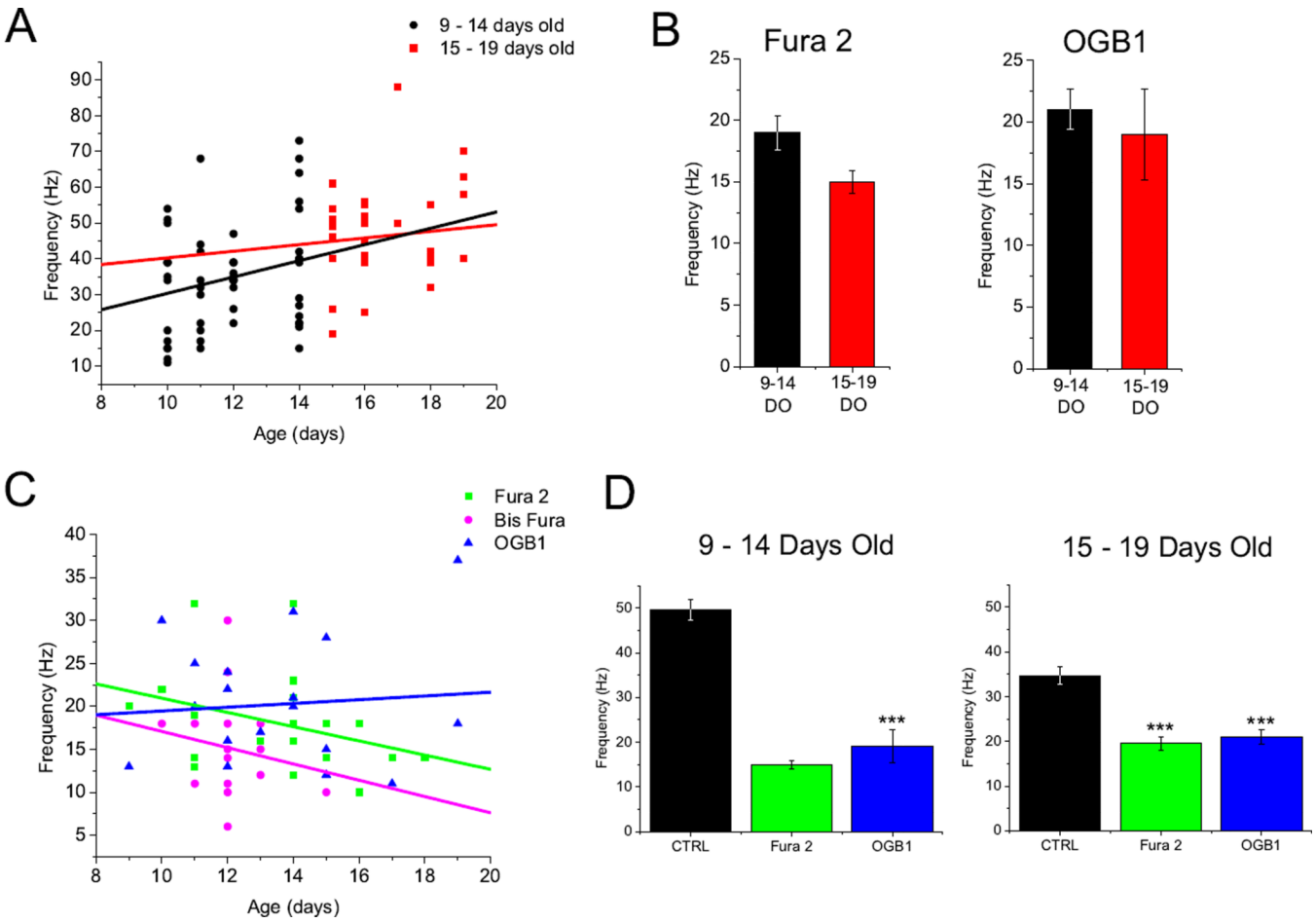

Fig. 7.

Calcium dyes slowed the peak oscillation frequency in cells and confounded age dependent frequency increases. A. Scatter plot of the peak oscillation frequency of each control cell from 9– 19 days old (DO). Cells were sub-divided into 9–14 DO (black) and 15–19 DO (red). Linear regression fits for each group (9–14 DO R^2=0.24; 15–19 DO R^2=0.08). B. Bar graph showing average peak frequency for Fura 2 and OGB1 cells divided into 9–14 DO and 15–19 DO age groups (Fura 2 9 −14 DO 19±1.4 Hz; 15 – 19 DO 15±0.94 Hz, P>0.05; OGB1 9 −14 DO 21±1.7 Hz; 15 – 19 DO 19±3.7 Hz, P>0.05). Bis Fura was not compared. C. Scatter plot showing the peak oscillation frequency for each individual cell from 9–19 DO. Straight lines correspond to linear regression fits of each dye group (Fura 2 R^2 = −0.34; Bis Fura R^2=−0.2; OGB1 R^2=0.08). D. Bar graph comparing average peak frequency of Fura 2 and OGB1 dye groups to control cells of equivalent age. Both dye groups showed significantly lower frequencies regardless of age (CTRL 9-14DO 34.6±2.1; Fura 2 vs. CTRL, P< 0.001; OGB1 vs. CTRL, P< 0.001; CTRL 15–19DO 49.5±2.4; Fura 2 vs. CTRL, P< 0.001; OGB1 vs. CTRL, P< 0.001)